Molecular Therapy
Nucleic Acids
Original Article

Proof of concept of peptide-linked blockmiR-induced MBNL functional rescue in myotonic dystrophy type 1 mouse model

Sarah J. Overby,[1,2] Estefanía Cerro-Herreros,[1,2] Irene González-Martínez,[1,2] Miguel A. Varela,[3,4] David Seoane-Miraz,[3,4] Yahya Jad,[3,4] Richard Raz,[3,4] Thorleif Møller,[5] Manuel Pérez-Alonso,[1,2] Matthew J. Wood,[3,4] Beatriz Llamusí,[1,2,6] and Rubén Artero[1,2]

[1]University Institute of Biotechnology and Biomedicine (BIOTECMED), Universidad de Valencia, 46100 Burjassot, Spain; [2]Translational Genomics Group, Incliva Biomedical Research Institute, 46010 Valencia, Spain; [3]Department of Paediatrics, University of Oxford, John Radcliffe Hospital, OX3 9DU Oxford, UK; [4]MDUK Oxford Neuromuscular Centre, University of Oxford, Oxford, UK; [5]Ranger Biotechnologies, Odense, Denmark

Myotonic dystrophy type 1 is a debilitating neuromuscular disease causing muscle weakness, myotonia, and cardiac dysfunction. The phenotypes are caused by muscleblind-like (MBNL) protein sequestration by toxic RNA in the DM1 protein kinase (*DMPK*) gene. DM1 patients exhibit a pathogenic number of repetitions in *DMPK*, which leads to downstream symptoms. Another disease characteristic is altered microRNA (miRNA) expression. It was previously shown that miR-23b regulates the translation of *MBNL1* into protein. Antisense oligonucleotide (AON) treatment targeting this miRNA can improve disease symptoms. Here, we present a refinement of this strategy targeting a miR-23b binding site on the *MBNL1* 3′ UTR in DM1 model cells and mice by using AONs called blockmiRs. BlockmiRs linked to novel cell-penetrating peptide chemistry showed an increase in MBNL1 protein in DM1 model cells and HSA^{LR} mice. They also showed an increase in muscle strength and significant rescue of downstream splicing and histological phenotypes in mice without disturbing the endogenous levels of other miR-23b target transcripts.

INTRODUCTION

Myotonic dystrophy type 1 (DM1) is a dominantly inherited neuromuscular disorder characterized by muscle weakness and involuntary muscle contraction. These symptoms have a significant impact in the quality of life of patients, especially when muscle strength is needed.[1] Other symptoms include cardiac arrhythmias, cataracts, insulin resistance, and respiratory difficulties (OMIM; MIM: 160900). The disease originates in a toxic CUG repeat expansion in the DM1 protein kinase (*DMPK*) gene transcripts inducing the sequestration of muscleblind-like (MBNL) proteins.[2] MBNL proteins play a critical role in regulating mRNA metabolism, specifically post-transcription alternative splicing and alternative polyadenylation.[3–5] MBNL1 and 2 have similar expression patterns post-natally, encouraging adult alternative splicing patterns. They also show functional overlap and can compensate for one another when necessary.[6] MBNL3 principally functions during the embryonic prenatal phase or in adult regenerating tissues. Consequently, aberrant fetal splicing patterns in certain transcripts are hallmarks of the DM1 disease profile and lead to the DM1 phenotype.[6] Indeed, human-induced pluripotent stem cells (hiPSCs) that were CRISPR-Cas9 edited to reduce MBNL proteins recapitulated DM1 phenotypes, such as mis-splicing and impairment of late myogenic fusion.[7]

In addition, as MBNL proteins are sequestered, CUGBP Elav-like family member 1 (CELF1) proteins are upregulated.[8] CELF1 proteins also function as splicing regulators, and their increase also contributes to splicing abnormalities in DM1. Indeed, CELF and MBNL proteins show an antagonistic relationship that effects splicing patterns.[9]

Antisense oligonucleotides (AONs) are a promising nucleic acid therapy across a variety of neuromuscular disorders.[10] Indeed, various AONs have also shown promise for treatment of DM1.[11] For example, short locked-nucleic acid (LNA), charge-neutral morpholino (PMO), and cell-penetrating peptide-linked morpholino (P-PMO)-based AONs targeting the toxic *DMPK* repetitions were able to block the binding of MBNL proteins.[12–14] Specifically, one P-PMO produced therapeutic results in DM1 HSA^{LR} mice, including splicing rescue, myotonia, and reduction of nuclear foci.[14]

PMOs have a neutral charge that create a highly stable compound and facilitate efficient delivery to the cell. A PMO called eteplirsen has already obtained US Food and Drug Administration (FDA) approval for the treatment of Duchenne muscular dystrophy (DMD).[15] PMOs can also be covalently linked with cell-penetrating peptides to further

Received 15 September 2021; accepted 6 February 2022;
https://doi.org/10.1016/j.omtn.2022.02.003.

[6]Present address: ARTHEx Biotech S.L., Calle Catedrático Agustín Escardino 9, 46980 Paterna, Spain

Correspondence: Ruben Artero, University Institute for Biotechnology and Biomedicine (BIOTECMED), Universidad de Valencia, 46100 Burjassot, Spain
E-mail: ruben.artero@uv.es

promote cell uptake like the Pip6a-PMO compound that previously showed cardiac improvements in DMD mouse models.[16,17] Pip6a-PMO has also been used for the treatment of DM1 by targeting the toxic repeat sequence in *DMPK*.[18]

AONs have recently been used in a novel therapeutic strategy in DM1 by targeting microRNAs (miRNAs) regulating MBNL protein synthesis instead of the CUG repetitions. In this way, increased MBNL production can compensate for non-functional MBNL sequestered by toxic repeats. It has been previously shown that antagomiRs targeting miR-218 and miR-23b increase MBNL1 production by blocking *MBNL* transcript regulation.[19] Rescue of MBNL1 protein was observed after treatment in DM1 cells[19] as well as in HSA^{LR} mice.[20] Other rescue observed in these studies include alternative splicing, histological phenotypes, myotonia, and grip strength. Concurrently, miRNA activity is increasingly being investigated in the context of DM1, namely the roles of miR-7[21] and miR-1.[22]

AntimiRs or "antagomiRs" have been well characterized for their capability in blocking miRNA activity.[23,24] However, because miRNAs can have hundreds of target transcripts,[25] it is difficult to set apart their specific effects on MBNLs versus their additional effects on several other mRNAs. In this paper, we describe an alternative to antimiR technology called "blockmiRs". BlockmiRs are similar to antimiRs in that they both use antisense technology to reduce miRNA regulation. However, instead of binding to miRNAs, they bind specifically to the 3′ untranslated region (UTR) binding site on the target transcript. This blocks interaction with miRNAs, thereby allowing translation to occur. In this way, blockmiRs are binding site sequence specific and not miRNA sequence specific.

BlockmiRs have already shown success in the study of angiogenesis. Concretely, miR-27a was identified as a regulator of VE-cadherin. miR-27a upregulation blocks capillary tube formation and angiogenesis. Therefore, a blockmiR was designed against the binding site of miR-27a on the VE-cadherin 3′ UTR.[26] When injected into mice after ischemic injury, the blockmiR blocked the regulation of miR-27a, which promoted the formation of new blood vessels and reduced vascular leak. After the proof of concept, the 2'-O-methyl-based blockmiR termed CD5-2 was tested in the context of diabetes-related retinal dysfunction, which breaks down the blood-retinal barrier and leads to retinal damage and inflammation and, in some cases, even blindness.[27] CD5-2 again reduced vascular leakage and inflammation in diabetic mouse models.

There is one confirmed binding site for miR-23b on the *MBNL1* 3′ UTR and one on the *MBNL2* 3′ UTR. There are three confirmed binding sites for miR-218 on the *MBNL2* 3′ UTR. In this study, a single blockmiR was designed to target the only binding site for miR-23b on the *MBNL1* 3′ UTR for proof of concept as DM1 therapy and for simplicity in interpreting results. Here, we show the effects of a novel blockmiR strategy in DM1 treatment with linkage to a new peptide called Pip9b2. The peptide is designed to facilitate efficient entry into the cell without the use of transfection reagents. Pip9b2 peptide-linked PMO blockmiRs were designed against a binding site of miR-23b on *MBNL1* and tested in immortalized patient-derived DM1 fibroblasts transdifferentiated into myotubes (DM1 cells).[28] After treatment in cells, the blockmiR increased the amount of *MBNL1* transcripts and protein with low toxicity. The compound was then effectively delivered to HSA^{LR} mice muscle with highly specific results. Therapeutic effects include increased grip strength, splicing rescue, increase in Mbnl1 protein, and histological improvements.

RESULTS

Pip9b2-linked PMO blockmiR increases MBNL1 in cells

Pip9b2 is a cell-penetrating peptide that contains two flanking regions enriched with arginines (cationic amino acids) and a central hydrophobic core. The sequence can be found in materials and methods. The peptide linkage to the PMO blockmiR is designed to facilitate cell entry without the need for transfection reagent. To test for cell toxicity, the P-PMO blockmiR and a peptide linked with a scrambled PMO (P-SC), a chemistry control, were administered in DM1 cells at increasing concentrations (Figure 1A). The peptide-linked oligos showed little to no cell growth inhibition across all concentrations, in contrast to those treated with transfection reagent, which began to show 50% cell growth inhibition after 50 nM. Therefore, for the rest of the experiments, P-PMO and P-SC were administered at 1 μM per manufacturer's recommendation.

DM1 cells showed an increase in *MBNL1* and *2* transcript expression levels after P-PMO blockmiR treatment (Figures 1B and 1C). Aberrant fetal splicing patterns in *MBNL1* and *NFIX* transcripts show a strong phenotype in DM1 cells.[3] Treatment with miR-23b targeting antagomiRs has previously shown rescue with these transcripts.[19,20] After treatment with the blockmiR, a slight but significant return to the adult splicing pattern was also observed (Figures 1D–1F). The cells also showed a striking increase in MBNL1 protein immunofluorescence through analysis of confocal microscopy images (Figure 1G). From a qualitative standpoint, the cells treated with cell-penetrating peptide blockmiRs were visibly more prolific and showed a large increase in MBNL1 fluorescence in the cytoplasm. Quantification of the mean pixel intensity for each cell confirmed this increase (Figure 1H).

miR-23b binding site is conserved in mice

The success of the blockmiRs *in vitro* led to *in vivo* testing in mice. But before this experiment could take place, the binding site of miR-23b needed to be confirmed in mouse. Site 1 on the *MBNL1* 3′ UTR has previously been confirmed in HeLa cells through dual luciferase assay.[19] This site shares sequence homology with site 2 of the two predicted miR-23b binding sites in mice save for one nucleotide (Figure 2A). To confirm these predicted sites, another luciferase assay was performed in mouse C2C12 cells using *Mbnl1* 3′ UTR constructs. Three reporter plasmids were generated, one containing the wild-type (WT) *Mbnl1*, one with deletion of the respective miR-23b seed region in the binding site (Del), and one with a complementary perfect

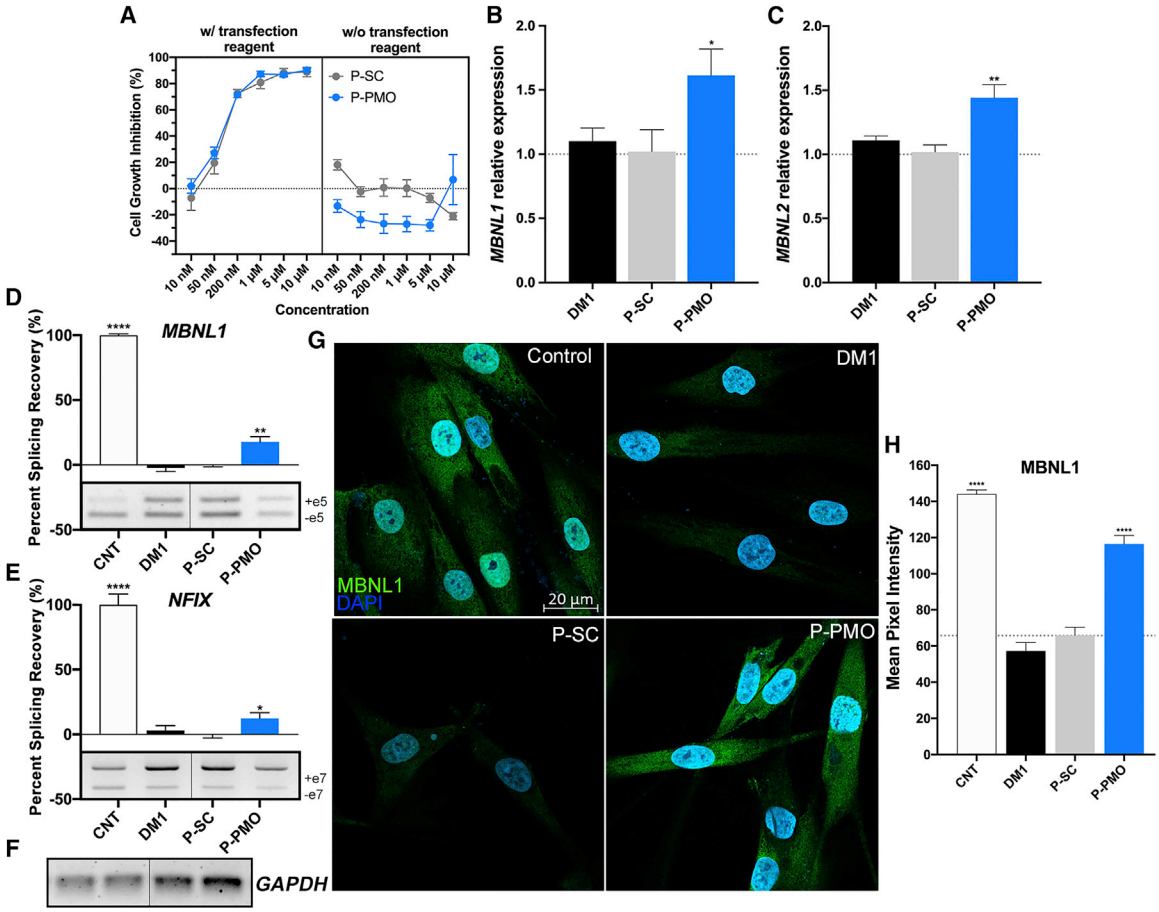

Figure 1. P-PMO blockmiR effects on DM1 cells

(A) The P-PMO blockmiR along with the scramble control (P-SC) was tested for cell viability at increasing concentrations with and without the use of transfection reagent. The peptide conjugation is designed to penetrate the cell without the need for transfection reagent. (B and C) Expression of (B) *MBNL1* and (C) *MBNL2* transcripts was relatively quantified in triplicate from cells after treatment with the P-PMO blockmiR and normalized to *GAPDH* endogenous expression. (D and E) Percent splicing recovery (PSR) was calculated through semiquantitative RT-PCR and exon band quantification for (D) *MBNL1* exon 5 and (E) *NFIX* exon 7 and normalized to CNT samples. Representative gels can be seen below each graph. (F) *GAPDH* was run as an endogenous control. (G and H) Immunofluorescence of MBNL1 protein (green) and DAPI (blue) was observed in DM1 and control cells (G) and the mean pixel intensity of each was quantified (H). Cell count: CNT n = 118, DM1 n = 83, P-SC n = 96, and P-PMO n = 108. All statistical comparisons were performed against P-SC via Student's t test. p value GraphPad (GP) style: p = 0.1234 (not significant [ns]), *p = 0.0332, **p = 0.0021, ***p = 0.0002, and ****p < 0.0001. Error bars represent SEM.

match (PM) to the full miR-23b sequence. The plasmids were transfected in C2C12 cells and the GLuc and SEAP luminescence was read after 48 h. If miRNA binding occurs, GLuc translation is inhibited and therefore luminescence decreases. SEAP is constitutively translated as a normalization control. Endogenous expression of miR-23b binding in the C2C12 cells was apparent through the increase of luminescence in the miR-23b binding site deletion plasmids in comparison to the WT (Figure 2B). In contrast, GLuc signal was decreased upon transfection with PM plasmids. This confirms that miR-23b is directly binding to these sites.

In order to further validate these binding sites, the experiment was repeated using a miR-23b mimic (Figure 2C). Upon seed region deletion, GLuc luminescence increased once again. Also supporting this information was the WT no-mimic control and the WT scrambled-mimic control, which both showed less miRNA repression compared with WT and mimic co-transfection. Through these assays, sites 1 and 2 were both confirmed as miR-23b binding sites in the mouse *Mbnl1* 3′ UTR. Therefore, P-PMO blockmiR was tested *in vivo* (Figure 2D). A new compound was generated, accounting for the single-nucleotide difference and was administered at 10 mg/kg through tail vein injection in HSA^{LR} DM1 model mice (n = 6). A scramble control was also injected at the same concentration (n = 6). A group of FVB healthy mice (n = 5) and a group of HSA^{LR} mice (n = 5) were administered PBS as two separate controls. After 4 days, mice were sacrificed and analyzed for disease phenotypes. This time period was chosen due to the strong amount of rescue seen in previous antagomiR studies in HSA^{LR} mice.[20,29]

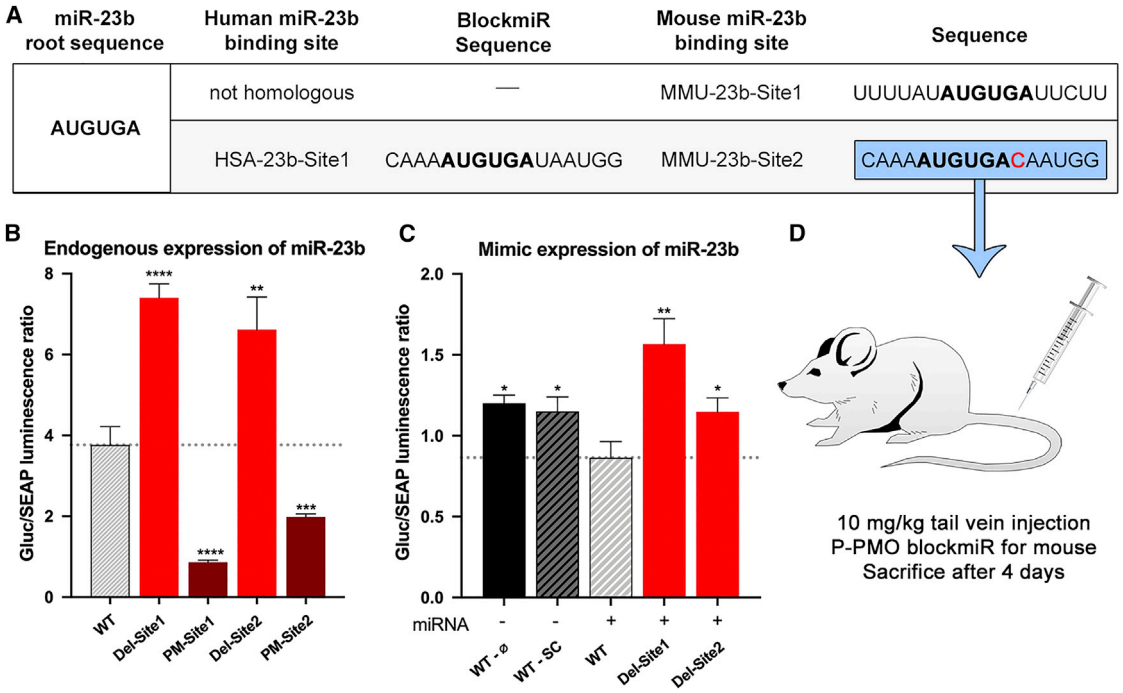

Figure 2. Dual luciferase assay confirms conservation of miR-23b binding site

(A) Sequence analysis (shown 5′ to 3′) shows that the predicted mouse site 2 is identical to human site 1 for miR-23b except for one nucleotide difference marked in red. miRNA seed region is marked in bold. (B) Gluc and SEAP luminescence was quantified in C2C12 mouse cells after transfection with reporter plasmids containing the 3′ UTR of Mbnl1 either wild type (WT), the miR-23b seed region deleted (Del), or perfect match (PM) to miR-23b. (C) To further confirm the luminescence observed was due to miR-23b, the experiment was repeated with co-transfection of a miRNA mimic of miR-23b. Two mimic controls were used: one with no mimic (WT-∅) and one with a scrambled mimic (WT-SC). All dual luciferase assays were normalized to SEAP and compared with WT for statistical comparison using Student's t test. p value GP style: p = 0.1234 (ns), *p = 0.0332, **p = 0.0021, ***p = 0.0002, and ****p < 0.0001. Error bars represent SEM. (D) After site confirmation, a new P-PMO blockmiR was generated, matching the mouse sequence along with a scramble control. They were administered by tail-vein injection at 10 mg/kg and left for 4 days before sacrifice and muscle isolation.

P-PMO increases grip strength and reaches disease-related tissues without off-target effects

Mice grip strength was measured before and after treatment, and the percent normal force was calculated for each group (Figure 3A). The P-PMO-treated mice showed a large increase in percentage of normal force. The change was statistically significant compared with the same mice treated with PBS through Student's t test. After treatment, blood serum was extracted from the mice for biochemical analysis (Figure 3B). The FVB levels were set as the healthy control level to which all other treatments were compared. Three parameters in HSA^{LR} mice treated with PBS were found to be significantly different from FVB levels, including amylase, aspartate aminotransferase (AST), and creatine phosphokinase (CPK). These parameters could be related to the disease phenotype; however, biochemical levels in HSA^{LR} have not been widely studied. Importantly, treatment with P-PMO and P-SC promoted a pattern more similar to FVB levels in amylase and AST. The only significant change from P-PMO or P-SC was a decrease in CPK levels after treatment with P-SC. CPK is released into the blood during muscle tissue damage.[30] The lower amounts seen here indicate a lack of tissue damage and are within the range for normal levels in healthy mice. In addition, P-SC and P-PMO showed no significant change in comparison to PBS controls. Importantly, the rest of the parameters indicating hepatotoxicity or tissue damage, including alanine transaminase (ALT), AST, bilirubin, bile acids, and lactic acid dehydrogenase (LDH), remained unchanged after blockmiR treatment. Other health indicators, such as creatinine, cholesterol, glucose, and triglycerides, as well as mouse weight were also stable.

BlockmiR concentration was quantified in skeletal and cardiac muscle by a custom ELISA assay (Figure 3C). Results showed highly efficient delivery with concentrations between 20 and 30 nM in heart, gastrocnemius, and quadriceps. Although the *hACTA1* gene is not expressed in cardiac tissue in HSA^{LR} mice, the efficient biodistribution of P-PMO in heart strongly suggests that the P-PMO could counteract other DM1-related symptoms, such as cardiac-conduction defects, which are the most common causes of death.[31]

Neither the P-PMO nor the scrambled control caused off-target changes on the relative levels of three miR-23b target transcripts (Figure 3D). *Cdk2*, *Met*, and *Tmem64* are all experimentally validated to be regulated by miR-23b according to miRDB[32] and strong evidence from miRTarBase.[33] Cyclin-dependent kinase 2 (*CDK2*), with validated miR-23b interaction by next-generation sequencing, codes for a protein kinase important for cell cycle regulation and plays a role

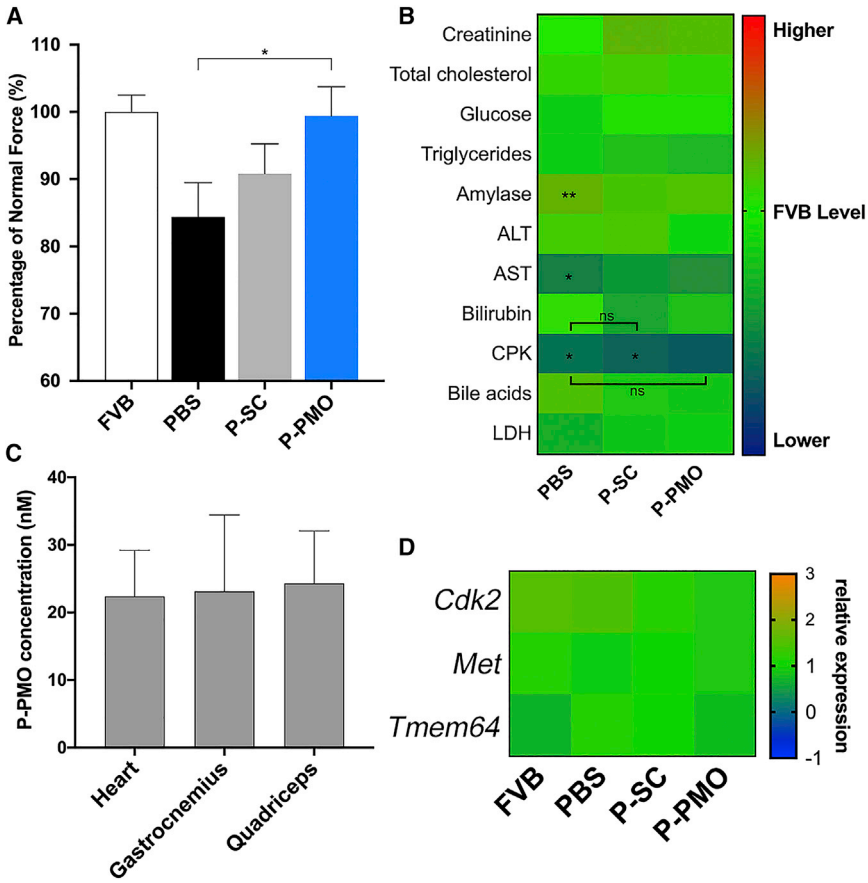

Figure 3. Pip9b2-linked blockmiR affects grip strength without toxicity

(A) Mouse grip strength was measured before and after treatment with P-PMO or P-SC by grip meter to calculate the percent of normal force normalized to mouse weight. (B) Blood serum biochemistry was analyzed after treatments. All samples in (B) were statistically compared with FVB mice through Kruskal-Wallis ANOVA and Wilcoxon test, if applicable. All parameters were within the normal range for healthy mice. Numerical values can be found in Table S2. (C) P-PMO biodistribution was quantified in mice heart, gastrocnemius, and quadriceps by ELISA using a specific phosphorothioate probe. (D) Relative expression of *Cdk2*, *Met*, and *Tmem64* transcripts was quantified in triplicate from quadriceps muscle after treatment with the blockmiR and normalized to *Gapdh* endogenous expression. Raw data values can be found in Table S3. All statistical comparisons in (A) and (D) were performed against P-SC via Student's t test. p value GP style: p = 0.1234 (ns), *p = 0.0332, **p = 0.0021, ***p = 0.0002, and ****p < 0.0001. Error bars represent SEM.

in activating DNA synthesis in human fibroblasts.[34] *MET*, validated by reporter assay, western blot, and qPCR, is a proto-oncogene that codes for a member of the receptor tyrosine kinase family of proteins. Alterations in expression levels of *MET* are associated with various human cancers.[35,36] Finally, transmembrane protein 64 (*TMEM64*), validated by reporter assay, western blot, and crosslinking immunoprecipitation sequencing (CLIP-seq), codes for a membrane protein that regulates Ca^{2+} signaling pathways, especially in osteoclasts. Interestingly, they work with the sarcoendoplasmic reticulum calcium transport ATPase (SERCA) family of proteins to maintain calcium transport homeostasis. ATP2A1 (also known as SERCA1) is a member of the SERCA family whose encoding transcript shows an aberrant fetal splicing pattern in DM1 patients.[37] In sum, *Cdk2*, *Met*, and *Tmem64* are protein-coding transcripts with important roles in proper cell function. These transcript levels were unaffected by P-PMO and P-SC treatment, which highlights the specificity of miR-23b binding site blocking.

BlockmiR induces rescue of HSA^{LR} mice phenotypes

After seeing promising results at the physiological level, the mice were analyzed at the molecular level for changes in the DM1 phenotype specifically in the quadriceps leg muscle. Transcripts *Atp2a1*, *Clcn1*, *Mbnl1*, and *Nfix* all show abnormal fetal-splicing patterns in the DM1 mice model.[38–41] Treatment with miR-23b targeting antagomiRs has previously shown rescue with these transcripts.[19,20] After blockmiR administration, correction was seen in all four transcripts (Figures 4A–4E). The percent splicing recovery compared with the P-SC control showed significant rescue.

The P-PMO also increased the amount of Mbnl1 protein (Figures 4F and 4G), in agreement with the increase in MBNL1 fluorescence seen previously in cell microscopy. Jess Simple Western technology was used to quantify the level of Mbnl1 normalized to the total protein level. The P-PMO showed significant increase compared with the P-SC and the HSA^{LR} PBS control.

Finally, a histological analysis was made of 10-μm sections of the quadriceps muscle (Figures 4H and 4I). After staining with hematoxylin and eosin, the percent of muscle fibers with central nuclei was quantified. The migration of muscle fiber nuclei toward the center of the muscle fibers is a well-known phenotype of HSA^{LR} mice muscle.[42] A significant decrease in the percent of fibers with central nuclei was observed in comparison to the P-SC samples. The P-PMO image in Figure 4I is representative of this rescue and shows a striking resemblance to the FVB sections. Nuclei quantification was done blindly after randomizing images to avoid bias. The error for nuclei quantifications was low for each individual mouse (Table S4).

DISCUSSION

A significant increase in MBNL1 protein was observed after treatment with P-PMO blockmiR through immunofluorescence in cells and Simple Western analysis in mice. Importantly, the treatment also did not over-rescue the abundance of

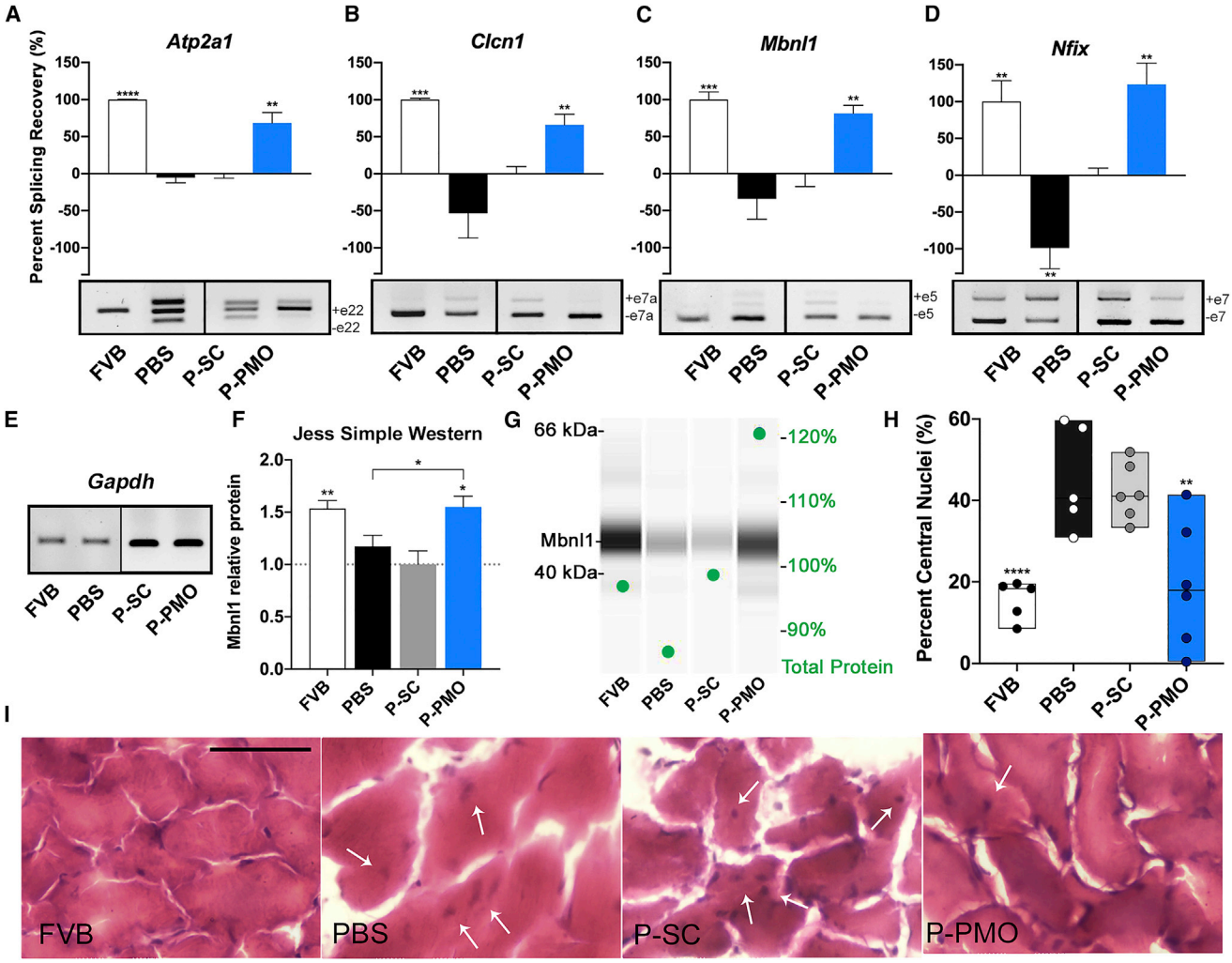

Figure 4. P-PMO blockmiR rescues molecular and histological phenotypes of HSA^{LR} mice

(A–D) Semiquantitative RT-PCR was performed to analyze alternative splicing patterns in exons of interest for (A) *Atp2a1*, (B) *Clcn1*, (C) *Mbnl1*, and (D) *Nfix* transcripts. (E) *Gapdh* was run as an endogenous control. PSR was calculated normalized to FVB samples. Representative gels can be seen below each graph. (F) Relative protein was quantified using Jess Simple Western technology. (G) A representative lane view shows the bands observed compared with total protein normalization (green dots and scale). Finally, 10-μm sections of quadriceps muscle were cut and stained with hematoxylin and eosin in order to visualize the localization of central nuclei within the muscle fibers. (H) An average of 500 fibers were analyzed per mouse. (I) Representative images of each treatment can be seen. Black scale bar represents 50 μm. The white arrows signal nuclei that have central localization. All samples were statistically compared with P-SC through Student's t test. p value GP style: p = 0.1234 (ns), *p = 0.0332, **p = 0.0021, ***p = 0.0002, and ****p < 0.0001. Error bars represent SEM.

MBNL1, as the levels reached were comparable to the healthy controls. The MBNL1 protein increase was also functional, as evidenced by the significant splicing rescue in cells and mice. MBNL proteins play a critical role in the alternative splicing patterns of the transcripts. Specifically, a recent study comparing mis-spliced transcripts in HSA^{LR} mice to Mbnl1$^{-/-}$ Mbnl2$^{+/-}$ knockout mice showed 81% overlap, which included *Atp2a1*, *Clcn1*, *Mbnl1*, and *Nfix*.[41] Indeed, *ATP2A1*, *MBNL1*, and *NFIX* splicing correction showed a dose response to MBNL1 knockout in human cells.[43] Likewise, *Clcn1* also shows response to *MBNL* knockout.[44] The results of P-PMO blockmiR treatment not only indicate an increase in MBNL1 protein, but the rescue of these four transcripts also indicates an upstream rescue of MBNL1 functionality.

These transcripts also play important roles in cell function. For example, *ATP2A1* codes for a key enzyme for Ca^{2+} metabolism in muscle cells.[45] *Mbnl1* ex5 splicing patterns are related to MBNL1 subcellular localization and functionality.[46] Furthermore, *Clcn1* mis-splicing is directly related to myotonia and muscle weakness.[47,48] Therefore, splicing rescue could be responsible for the increase in mice grip strength in this experiment. Other DM1 phenotypes,

such as myotonia, should be analyzed for therapeutic effects in future P-PMO blockmiR treatment.

One of the principal delimiting factors in antisense therapy is transporting the AONs across the cell membrane barrier.[49] In an experiment testing the cell membrane of HSA^{LR} mice, it was concluded that their cell membranes have a fully functional barrier.[50] Therefore, all AON treatments in DM1 must consider the integrity of the cell. The ELISA biodistribution quantification seen here in mice suggests that the cell-penetrating peptides are indeed capable of crossing the cell membrane. The successful delivery of the P-PMO in the quadriceps muscle can be directly observed through the decrease in the abundance of central nuclei and splicing correction. Although the exact degree to which the Pip9b favors the entry into the muscles is not quantified, the aforementioned therapeutic observations suggest that it is being delivered in much higher quantity than a naked PMO. In addition, the peptide technology did not cause any toxic effects *in vitro* or *in vivo*. Concretely, the P-PMO showed no off-target effects in regard to three miR-23b transcripts as well as biochemical panels. This is a critical advantage for the P-PMO design and chemistry and merits further *in vivo* study that could potentially be applied to other antisense treatment strategies.

Finally, the results seen in this study confirm the concept of blockmiR therapy in DM1. Indeed, the site-specific strategy showed similar therapeutic results to miRNA-specific antagomiR strategies.[19,29] Both strategies are capable of increasing MBNL1 protein and grip strength in HSA^{LR} mice as well as inducing therapeutic splicing alterations. In Cerro-Herreros et al.,[20] antagomiR-23b administered at 12.5 mg/kg and left for 4 days significantly increased the amount of Mbnl1 protein. While antagomiR-23b had stronger protein rescue, the P-PMO blockmiR seen here was able to make stronger recoveries in splicing, even at 10 mg/kg.

It has recently been shown that miR-218 is over-expressed in HSA^{LR} mice and DM1 patient-derived myotubes and biopsies.[29] The role of miRNAs is becoming increasingly implicated in the intricacies of the DM1 phenotype. The blockmiR technology presented here therefore merits further exploration now that proof of concept has been shown. Optimization of dosage and time response of the blockmiR will bring the cell-penetrating peptide technology to its highest potential.

MATERIALS AND METHODS

P-PMO blockmiR design

Phosphorodiamidate morpholino oligonucleotides (PMOs) are non-ionic oligonucleotides since the phosphodiester bonds are replaced by phosphoroamidite linkages and the riboses by morpholino moieties. The PMO blockmiR contains the following sequence: 5′-CCAUUAU CACAUUUUGCUCUU-3′. It is covalently linked to the cationic peptide Pip9b2: RXRRBRR FQILY RBRXRB (X, aminohexanoic acid; B, β-alanine). Peptides were synthesized and conjugated to PMOs as described previously.[51] A negative scrambled control Pip9b2-PMO was also generated with the following PMO sequence: 5′-TCTTACCT CAGTTACAATTTA-3′. Conjugates were centrifuged through 3k Amicon filters followed by filtration through 0.22 μm. Quality control was performed after each of the conjugations (high-performance liquid chromatography [HPLC]: >99%; MALDI-TOF: acceptance error of molecular weight is 0.1%). Following each freeze thaw cycle, peptide-PMOs are vortexed briefly and incubated for 30 min in a 37°C water bath. Subsequently, peptide-PMOs are sonicated for 30 s with a probe sonicator or 5 min with a water bath sonicator.

Cell culture

Healthy immortalized control-derived fibroblasts (CNT) and immortalized patient-derived fibroblasts carrying 1,300 CTG repeats (DM1) were provided by Dr. Furling[28] (Institute of Myology, Paris) and were transdifferentiated into myotubes by inducing MyoD expression. The fibroblasts were grown in DMEM with 4.5 g/L glucose, 1% penicillin and streptomycin (P/S), and 10% fetal bovine serum (FBS) (Sigma). Transdifferentiation was prompted by muscle differentiation medium (MDM) containing DMEM with 4.5 g/L glucose, 1% P/S, 2% horse serum, 1% apo-transferrin (10 mg/mL), 0.1% insulin (10 mg/mL), and 0.02% doxycycline (10 mg/mL). C2C12 cells were also grown in DMEM with 4.5 g/L glucose, 1% P/S, and 10% FBS (Sigma). All cells were grown at 37°C in a humidified atmosphere containing 5% CO_2.

Toxicity assay

Immortalized DM1 fibroblasts were plated in a 96-well plate (Falcon) at a concentration of 1.0×10^5 cells per mL. After 24 h, P-PMO blockmiRs and P-SC were transfected at 10 nM, 50 nM, 200 nM, 1 μM, 5 μM, and 10 μM in triplicate in MDM with X-tremeGENE HP DNA Transfection Reagent (Roche) according to manufacturer instructions and transdifferentiated into myotubes for 4 days. The same experiment was duplicated without the use of transfection reagent. To measure cell viability, 20 μL of MTS/phenazine methosulfate (PMS) tetrazolium salt from the CellTiter 96 Aqueous Non-Radioactive Cell Proliferation Assay (Promega) was added to each well and cells were incubated for 4 h at 37°C in a humidified chamber with 5% CO_2. The conversion of MTS into soluble formazan was measured by absorbance at 490 nm using an Infinite 200 PRO plate reader (Tecan). Data were normalized to non-transfected DM1 controls.

Cell transfection

DM1 cells and CNT cells were plated at 1.0×10^5 cells per mL in 10 mL Petri dishes (Falcon). DM1 cells were transfected with 1 μM of P-PMO or P-SC and transdifferentiated with MDM. CNT cells and DM1 cells treated with PBS were used as controls. The cells were left 4 days to transdifferentiate into myotubes.

Immunofluorescence

Immortalized DM1 fibroblasts were seeded at 4.0×10^4 cells per well in a 24-well plate (Falcon). After transfection and 4 days of differentiation, the transdifferentiated myotubes were fixed with 4% paraformaldehyde (PFA) for 15 min at room temperature (RT) and washed three times with 1× PBS. Myotubes were permeabilized with PBS-T (0.3% Triton-X in PBS) and blocked (PBS-T, 0.5% BSA, and 1% donkey serum) for 30 min at RT. They were then incubated with MBNL1 primary antibody (1:200, MB1a [4A8], Developmental

Studies Hybridoma Bank[52]) at 4°C overnight. After three PBS-T washes, the cells were incubated for 1 h with a biotinylated anti-mouse-immunoglobulin G (IgG) (1:200, Sigma-Aldrich) and subsequent Avidin-Biotin amplification (Elite ABC kit, VECTASTAIN) for 30 min at RT. They were followed by three PBS-T washes and incubation with streptavidin-fluorescein isothiocyanate (FITC) fluorophore (1:200, Vector) for 2 h at RT. After three washes with PBS, the cells were mounted with VECTASHIELD mounting medium containing 2 μg/mL DAPI (Vector) to detect the nuclei.

Images of DM1 cells were taken on an Olympus FluoView FV100 confocal microscope. The images were taken at a 40× magnification and quantified using ImageJ with the following formula at a threshold of 10: mean pixel intensity = gray value/area.

Dual luciferase assay

Luminescence of Gaussian luciferase (GLuc) and alkaline phosphatase (SEAP) were measured using the secreted-pair dual luminescence kit (GeneCopoeia) according to the manufacturer's protocols. Gaussian luciferase activity was normalized to alkaline phosphatase activity (GLuc/SEAP). Luminescence was measured using a Tecan Infinite M200 PRO plate reader (Life Sciences). Mbnl1 3′ UTR reporter pEZX-MT05 plasmids were designed containing WT Mbnl1, deletion of miR-23b seed region (Del), and PM of the full miR-23b sequence. The plasmids were transfected in C2C12 cells, and their luminescence was measured. The same assay was repeated with C2C12 cells co-transfected with miR-23b mimic, scrambled mimic, and no mimic controls. Full plasmid sequences can be found in the supplemental information appendix.

RNA extraction, qRT-PCR, and semiquantitative RT-PCR

Total RNA was isolated from transdifferentiated myotubes or gastrocnemius muscle using QIAzol Lysis Reagent and RNeasy Mini Kit (Qiagen) following manufacturer's recommendations. One microgram of RNA was digested with DNase (Zymo) and reverse transcribed with SuperScript II Reverse Transcriptase (Invitrogen) using random hexanucleotides (Roche).

Quantitative PCR was performed using approximately 4 ng of template cDNA from muscle cells with TaqMan probes (Qiagen) for *MBNL1* and *MBNL2* with FAM-labeled probes and *GAPDH* as an endogenous control with MAX-labeled probes. Quantitative PCR was performed for miR-23b targets *Cdk2*, *Met*, *Tmem64*, and *Gapdh* using approximately 4 ng of template cDNA from mice tissue with EvaGreen HOT FIREPol (Solis Biodyne). Three technical replicates were performed for each sample. Expression levels were measured using an Applied Biosystems StepOnePlus Real Time PCR System. Samples were normalized to *GAPDH/Gapdh* and calibrated with the P-SC control group using the $2^{-\Delta\Delta Ct}$ method. Samples were compared with P-SC using Student's t test applying Welch's correction when necessary.

Alternative splicing was analyzed using approximately 200 ng of cDNA in a standard PCR reaction with GoTaq polymerase (Promega). *MBNL1*- and *NFIX*-specific primers were used to analyze splicing patterns for cells cDNA, and *Atp2a1*-, *Clcn1*-, *Mbnl1*-, and *Nfix*-specific primers were for mouse cDNA (Table S1). *GAPDH* and a no reverse transcriptase (NRT) were run as cDNA controls (Figures S1 and S2). PCR products were run on a 2% agarose gel and the exons quantified with ImageJ software (NIH). Percentage splice recovery (PSR) index was defined as value%$_{SI}$ minus $\overline{X}\%_{DSI}$, divided by $\overline{X}\%_{DSI}$ minus $\overline{X}\%_{HSI}$ (where SI is splicing inclusion of each sample, DSI is disease splicing inclusion, and HSI is healthy splicing inclusion). Samples were compared with P-SC using Student's t test applying Welch's correction when necessary.

Transgenic mice and blockmiR administration

Mouse handling and experimental procedures conformed to the European law regarding laboratory animal care and experimentation (2003/65/CE) and were approved by the Conselleria de Agricultura, Generalitat Valenciana ("Respuesta terapéutica a blockmiRs modificados en un modelo de ratón de DM1"; reference number 2020/VSC/PEA/0203). Homozygous transgenic HSA^{LR} (line 20 b) mice[42] were provided by Prof. C. Thornton (University of Rochester Medical Center, Rochester, NY, USA), and mice with the corresponding genetic background (FVB) were used as controls. Age-matched HSA^{LR} (∼3.5 months old) mice received one intravenous tail vein injection of 150 μL of either 1× PBS (n = 5), P-PMO 10 mg/kg (n = 6), or P-SC 10 mg/kg (n = 6), and FVB mice of the same age also received one intravenous tail vein injection of 150 μL of 1× PBS (n = 5). Four days after injection, the mice were sacrificed, and blood, muscles, and organs of interest were extracted. Muscles were divided into two tubes: one part was frozen in liquid nitrogen for the molecular analyses and the other was fixed with −80°C chilled isopentane before histological processing.

Forelimb grip strength test

The forelimb grip strength was measured with a Grip Strength Meter (BIO-GS3; Bioseb, USA). The peak pull force (measured in grams) was recorded on a digital force transducer when the mouse grasped the bar. The gauge of force transducer was reset to 0 g after each measurement. Tension was recorded by the gauge at the time the mouse released its forepaws from the bar. The measurement was performed three consecutive times at 30-s intervals. The body weight measurement was performed in parallel. Percentage of normal force was calculated by normalizing the average strength after treatment to the strength before treatment and dividing this value by the body weight of each mouse.

Blood biochemistry

Blood serum was collected for each mouse and analyzed for biochemical parameters by Laboratorios Montoro Botella (Valencia, Spain). All samples were statistically compared with FVB mice through Kruskal-Wallis ANOVA and Wilcoxon test, if applicable.

ELISA oligonucleotide biodistribution

ELISA-based quantification of oligonucleotide biodistribution was performed as described in Burki et al.[53] using a phosphorothioate

(*) probe (sequence [5′/3′] [DIG] A*A*G*A*G*C*A*A*A*A*T*G*T*G*A*T*A*A*T*G*G [BIO]) double labeled with digoxigenin and biotin. This probe was used to detect the P-PMO in heart, gastrocnemius, and quadriceps from treated HSA^{LR} mice.

Protein extraction and Jess Simple Western

For total protein extraction, human DM1 cells or mouse tissues were sonicated and homogenized in Pierce RIPA buffer (Thermo Scientific) supplemented with protease and phosphatase inhibitor cocktails (Roche Applied Science). Quantification of total protein was performed with a BCA protein assay kit (Pierce) using BSA as standard. For the immunodetection assay in mouse tissues, the Jess Simple Western system was used to quantify Mbnl1 protein chemiluminescence (1:50, MB1a [4A8], Developmental Studies Hybridoma Bank[52]) and normalized to total protein fluorescence.

Muscle histology

Frozen 10-μm sections of mouse quadriceps muscles were stained with hematoxylin and eosin and mounted with VECTASHIELD mounting medium (Vector) according to standard procedures. Images were taken at a 100× magnification with a Leica DM2500 microscope. The percentage of fibers containing central nuclei was quantified in an average of 500 fibers in each mouse. All images were labeled randomly during quantification to facilitate a blind analysis. Whole sections can be found in Figure S3.

Statistical analysis

All statistical analyses were performed using Prism 8.2.1 (GraphPad) with special assistance from Dr. Juan Carbonell (Biostatistician, INCLIVA, Valencia, Spain).

SUPPLEMENTAL INFORMATION

Supplemental information can be found online at https://doi.org/10.1016/j.omtn.2022.02.003.

ACKNOWLEDGMENTS

This project was funded by the Myotonic Dystrophy Foundation (MDF) and the Tatami project funded by "La Caixa" Banking Foundation under the project code HR17-00268. Additional funding was from the PROMETEO/2020/081 project granted by the Conselleria d'Innovació, Universitats, Ciència i Societat Digital (Generalitat Valenciana). Part of the equipment employed in this work has been funded by Generalitat Valenciana and co-financed with ERDF funds (OP ERDF of Comunitat Valenciana 2014-2020). S.J.O. was funded by Santiago Grisolía code GRISOLIAP/2017/015. Special thanks to Developmental Studies Hybridoma Bank for the MB1a antibodies and to Arantxa García Redón for research assistance.

AUTHOR CONTRIBUTIONS

S.J.O., E.C.-H., I.G.-M., B.L., and D.S.-M. performed research; S.J.O., R.A., and B.L. designed research; M.A.V., Y.J., and R.R. provided the compounds; R.A., M.J.W., and M.P.-A. contributed to conceptualization and funding acquisition; and S.J.O. analyzed data and wrote the paper.

DECLARATION OF INTERESTS

We declare that R.A., B.L., and E.C.-H. are co-inventors in patent PCT/EP2017/073685, currently licensed to Arthex Biotech, of which R.A. and B.L. are co-founders and R.A. is scientific consultant.

REFERENCES

1. Landfeldt, E., Nikolenko, N., Jimenez-Moreno, C., Cumming, S., Monckton, D.G., Faber, C.G., Merkies, I.S.J., Gorman, G., Turner, C., and Lochmuller, H. (2020). Activities of daily living in myotonic dystrophy type 1. Acta Neurol. Scand. *141*, 380–387.
2. Miller, J.W., Urbinati, C.R., Teng-Umnuay, P., Stenberg, M.G., Byrne, B.J., Thornton, C.A., and Swanson, M.S. (2000). Recruitment of human muscleblind proteins to (CUG)(n) expansions associated with myotonic dystrophy. EMBO J. *19*, 4439–4448.
3. Konieczny, P., Stepniak-Konieczna, E., and Sobczak, K. (2014). MBNL proteins and their target RNAs, interaction and splicing regulation. Nucleic Acids Res. *42*, 10873–10887.
4. Konieczny, P., Stepniak-Konieczna, E., and Sobczak, K. (2017). MBNL expression in autoregulatory feedback loops. RNA Biol. 1–8.
5. Batra, R., Charizanis, K., Manchanda, M., Mohan, A., Li, M., Finn, D.J., Goodwin, M., Zhang, C., Sobczak, K., Thornton, C.A., et al. (2014). Loss of MBNL leads to disruption of developmentally regulated alternative polyadenylation in RNA-mediated disease. Mol. Cell *56*, 311–322.
6. Sznajder, L.J., and Swanson, M.S. (2019). Short tandem repeat expansions and RNA-mediated pathogenesis in myotonic dystrophy. Int. J. Mol. Sci. *20*, 3365.
7. Merien, A., Tahraoui-Bories, J., Cailleret, M., Dupont, J.B., Leteur, C., Polentes, J., Carteron, A., Polveche, H., Concordet, J.P., Pinset, C., et al. (2021). CRISPR gene editing in pluripotent stem cells reveals the function of MBNL proteins during human in vitro myogenesis. Hum. Mol. Genet. *31*, 41–56.
8. Wheeler, T.M., and Thornton, C.A. (2007). Myotonic dystrophy: RNA-mediated muscle disease. Curr. Opin. Neurol. *20*, 572–576.
9. Wang, E.T., Ward, A.J., Cherone, J.M., Giudice, J., Wang, T.T., Treacy, D.J., Lambert, N.J., Freese, P., Saxena, T., et al. (2015). Antagonistic regulation of mRNA expression and splicing by CELF and MBNL proteins. Genome Res. *25*, 858–871.
10. Rinaldi, C., and Wood, M.J.A. (2018). Antisense oligonucleotides: the next frontier for treatment of neurological disorders. Nat. Rev. Neurol. *14*, 9–21.
11. Xiong, H., Veedu, R.N., and Diermeier, S.D. (2021). Recent advances in oligonucleotide therapeutics in oncology. Int. J. Mol. Sci. *22*, 3295.
12. Wojtkowiak-Szlachcic, A., Taylor, K., Stepniak-Konieczna, E., Sznajder, L.J., Mykowska, A., Sroka, J., Thornton, C.A., and Sobczak, K. (2015). Short antisense-locked nucleic acids (all-LNAs) correct alternative splicing abnormalities in myotonic dystrophy. Nucleic Acids Res. *43*, 3318–3331.
13. Wheeler, T.M., Sobczak, K., Lueck, J.D., Osborne, R.J., Lin, X., Dirksen, R.T., and Thornton, C.A. (2009). Reversal of RNA dominance by displacement of protein sequestered on triplet repeat RNA. Science *325*, 336–339.
14. Leger, A.J., Mosquea, L.M., Clayton, N.P., Wu, I.H., Weeden, T., Nelson, C.A., Phillips, L., Roberts, E., Piepenhagen, P.A., Cheng, S.H., et al. (2013). Systemic delivery of a Peptide-linked morpholino oligonucleotide neutralizes mutant RNA toxicity in a mouse model of myotonic dystrophy. Nucleic Acid Ther. *23*, 109–117.
15. Lim, K.R., Maruyama, R., and Yokota, T. (2017). Eteplirsen in the treatment of Duchenne muscular dystrophy. Drug Des. Devel Ther. *11*, 533–545.
16. Blain, A.M., Greally, E., McClorey, G., Manzano, R., Betts, C.A., Godfrey, C., O'Donovan, L., Coursindel, T., Gait, M.J., Wood, M.J., et al. (2018). Peptide-conjugated phosphodiamidate oligomer-mediated exon skipping has benefits for cardiac function in mdx and Cmah-/-mdx mouse models of Duchenne muscular dystrophy. Plos One *13*, e0198897.
17. Forand, A., Muchir, A., Mougenot, N., Sevoz-Couche, C., Peccate, C., Lemaitre, M., Izabelle, C., Wood, M., Lorain, S., and Pietri-Rouxel, F. (2020). Combined treatment with peptide-conjugated phosphorodiamidate morpholino oligomer-PPMO and AAV-U7 rescues the severe DMD phenotype in mice. Mol. Ther. Methods Clin. Dev. *17*, 695–708.

18. Klein, A.F., Varela, M.A., Arandel, L., Holland, A., Naouar, N., Arzumanov, A., Seoane, D., Revillod, L., Bassez, G., Ferry, A., et al. (2019). Peptide-conjugated oligonucleotides evoke long-lasting myotonic dystrophy correction in patient-derived cells and mice. J. Clin. Invest *129*, 4739–4744.

19. Cerro-Herreros, E., Sabater-Arcis, M., Fernandez-Costa, J.M., Moreno, N., Perez-Alonso, M., Llamusi, B., and Artero, R. (2018). miR-23b and miR-218 silencing increase Muscleblind-like expression and alleviate myotonic dystrophy phenotypes in mammalian models. Nat. Commun. *9*, 2482.

20. Cerro-Herreros, E., Gonzalez-Martinez, I., Moreno-Cervera, N., Overby, S., Perez-Alonso, M., Llamusi, B., and Artero, R. (2020). Therapeutic potential of AntagomiR-23b for treating myotonic dystrophy. Mol. Ther. Nucleic Acids *21*, 837–849.

21. Sabater-Arcis, M., Bargiela, A., Furling, D., and Artero, R. (2020). miR-7 restores phenotypes in myotonic dystrophy muscle cells by repressing hyperactivated autophagy. Mol. Ther. Nucleic Acids *19*, 278–292.

22. Rau, F., Freyermuth, F., Fugier, C., Villemin, J.P., Fischer, M.C., Jost, B., Dembele, D., Gourdon, G., Nicole, A., Duboc, D., et al. (2011). Misregulation of miR-1 processing is associated with heart defects in myotonic dystrophy. Nat. Struct. Mol. Biol. *18*, 840–845.

23. Lopez Castel, A., Overby, S.J., and Artero, R. (2019). MicroRNA-based therapeutic perspectives in myotonic dystrophy. Int. J. Mol. Sci. *20*, 5600.

24. Rupaimoole, R., and Slack, F.J. (2017). MicroRNA therapeutics: towards a new era for the management of cancer and other diseases. Nat. Rev. Drug Discov. *16*, 203–222.

25. Bartel, D.P. (2009). MicroRNAs: target recognition and regulatory functions. Cell *136*, 215–233.

26. Young, J.A., Ting, K.K., Li, J., Moller, T., Dunn, L., Lu, Y., Moses, J., Prado-Lourenco, L., Khachigian, L.M., Ng, M., et al. (2013). Regulation of vascular leak and recovery from ischemic injury by general and VE-cadherin-restricted miRNA antagonists of miR-27. Blood *122*, 2911–2919.

27. Ting, K.K., Zhao, Y., Shen, W., Coleman, P., Yam, M., Chan-Ling, T., Li, J., Moller, T., Gillies, M., Vadas, M.A., et al. (2019). Therapeutic regulation of VE-cadherin with a novel oligonucleotide drug for diabetic eye complications using retinopathy mouse models. Diabetologia *62*, 322–334.

28. Arandel, L., Polay Espinoza, M., Matloka, M., Bazinet, A., De Dea Diniz, D., Naouar, N., Rau, F., Jollet, A., Edom-Vovard, F., Mamchaoui, K., et al. (2017). Immortalized human myotonic dystrophy muscle cell lines to assess therapeutic compounds. Dis. Model Mech. *10*, 487–497.

29. Cerro-Herreros, E., Gonzalez-Martinez, I., Moreno, N., Espinosa-Espinosa, J., Fernandez-Costa, J.M., Colom-Rodrigo, A., Overby, S.J., Seoane-Miraz, D., Poyatos-Garcia, J., Vilchez, J.J., et al. (2021). Preclinical characterization of antagomiR-218 as a potential treatment for myotonic dystrophy. Mol. Ther. Nucleic Acids *26*, 174–191.

30. Veenstra, J., Smit, W.M., Krediet, R.T., and Arisz, L. (1994). Relationship between elevated creatine phosphokinase and the clinical spectrum of rhabdomyolysis. Nephrol. Dial Transpl. *9*, 637–641.

31. Ashizawa, T., Gagnon, C., Groh, W.J., Gutmann, L., Johnson, N.E., Meola, G., Moxley, R., 3rd, Pandya, S., Rogers, M.T., Simpson, E., et al. (2018). Consensus-based care recommendations for adults with myotonic dystrophy type 1. Neurol. Clin. Pract. *8*, 507–520.

32. Chen, Y., and Wang, X. (2020). miRDB: an online database for prediction of functional microRNA targets. Nucleic Acids Res. *48*, D127–D131.

33. Huang, H.Y., Lin, Y.C., Li, J., Huang, K.Y., Shrestha, S., Hong, H.C., Tang, Y., Chen, Y.G., Jin, C.N., Yu, Y., et al. (2020). miRTarBase 2020: updates to the experimentally validated microRNA-target interaction database. Nucleic Acids Res. *48*, D148–D154.

34. Pagano, M., Pepperkok, R., Lukas, J., Baldin, V., Ansorge, W., Bartek, J., and Draetta, G. (1993). Regulation of the cell cycle by the cdk2 protein kinase in cultured human fibroblasts. J. Cell Biol *121*, 101–111.

35. Wu, X., Cheng, Y.L., Matthen, M., Yoon, A., Schwartz, G.K., Bala, S., Taylor, A.M., and Momen-Heravi, F. (2021). Down-regulation of the tumor suppressor miR-34a contributes to head and neck cancer by up-regulating the MET oncogene and modulating tumor immune evasion. J. Exp. Clin. Cancer Res. *40*, 70.

36. Moosavi, F., Giovannetti, E., Saso, L., and Firuzi, O. (2019). HGF/MET pathway aberrations as diagnostic, prognostic, and predictive biomarkers in human cancers. Crit. Rev. Clin. Lab Sci. *56*, 533–566.

37. Hino, S., Kondo, S., Sekiya, H., Saito, A., Kanemoto, S., Murakami, T., Chihara, K., Aoki, Y., Nakamori, M., Takahashi, M.P., et al. (2007). Molecular mechanisms responsible for aberrant splicing of SERCA1 in myotonic dystrophy type 1. Hum. Mol. Genet. *16*, 2834–2843.

38. Du, H., Cline, M.S., Osborne, R.J., Tuttle, D.L., Clark, T.A., Donohue, J.P., Hall, M.P., Shiue, L., Swanson, M.S., Thornton, C.A., et al. (2010). Aberrant alternative splicing and extracellular matrix gene expression in mouse models of myotonic dystrophy. Nat. Struct. Mol. Biol. *17*, 187–193.

39. Dixon, D.M., Choi, J., El-Ghazali, A., Park, S.Y., Roos, K.P., Jordan, M.C., Fishbein, M.C., Comai, L., and Reddy, S. (2015). Loss of muscleblind-like 1 results in cardiac pathology and persistence of embryonic splice isoforms. Sci. Rep. *5*, 9042.

40. Lin, X., Miller, J.W., Mankodi, A., Kanadia, R.N., Yuan, Y., Moxley, R.T., Swanson, M.S., and Thornton, C.A. (2006). Failure of MBNL1-dependent post-natal splicing transitions in myotonic dystrophy. Hum. Mol. Genet. *15*, 2087–2097.

41. Tanner, M.K., Tang, Z., and Thornton, C.A. (2021). Targeted splice sequencing reveals RNA toxicity and therapeutic response in myotonic dystrophy. Nucleic Acids Res. *49*, 2240–2254.

42. Mankodi, A., Logigian, E., Callahan, L., McClain, C., White, R., Henderson, D., Krym, M., and Thornton, C.A. (2000). Myotonic dystrophy in transgenic mice expressing an expanded CUG repeat. Science *289*, 1769–1773.

43. Wagner, S.D., Struck, A.J., Gupta, R., Farnsworth, D.R., Mahady, A.E., Eichinger, K., Thornton, C.A., Wang, E.T., and Berglund, J.A. (2016). Dose-dependent regulation of alternative splicing by MBNL proteins reveals biomarkers for myotonic dystrophy. Plos Genet. *12*, e1006316.

44. Choi, J., Personius, K.E., DiFranco, M., Dansithong, W., Yu, C., Srivastava, S., Dixon, D.M., Bhatt, D.B., Comai, L., Vergara, J.L., et al. (2015). Muscleblind-like 1 and muscleblind-like 3 depletion synergistically enhances myotonia by altering clc-1 RNA translation. EBioMedicine *2*, 1034–1047.

45. Vihola, A., Sirito, M., Bachinski, L.L., Raheem, O., Screen, M., Suominen, T., Krahe, R., and Udd, B. (2013). Altered expression and splicing of Ca(2+) metabolism genes in myotonic dystrophies DM1 and DM2. Neuropathol. Appl. Neurobiol. *39*, 390–405.

46. Terenzi, F., and Ladd, A.N. (2010). Conserved developmental alternative splicing of muscleblind-like (MBNL) transcripts regulates MBNL localization and activity. RNA Biol. *7*, 43–55.

47. Tang, Z.Z., Yarotskyy, V., Wei, L., Sobczak, K., Nakamori, M., Eichinger, K., Moxley, R.T., Dirksen, R.T., and Thornton, C.A. (2012). Muscle weakness in myotonic dystrophy associated with misregulated splicing and altered gating of Ca(V)1.1 calcium channel. Hum. Mol. Genet. *21*, 1312–1324.

48. Wheeler, T.M., Lueck, J.D., Swanson, M.S., Dirksen, R.T., and Thornton, C.A. (2007). Correction of ClC-1 splicing eliminates chloride channelopathy and myotonia in mouse models of myotonic dystrophy. J. Clin. Invest *117*, 3952–3957.

49. Crooke, S.T., Wang, S., Vickers, T.A., Shen, W., and Liang, X.H. (2017). Cellular uptake and trafficking of antisense oligonucleotides. Nat. Biotechnol. *35*, 230–237.

50. Gonzalez-Barriga, A., Kranzen, J., Croes, H.J., Bijl, S., van den Broek, W.J., van Kessel, I.D., van Engelen, B.G., van Deutekom, J.C., Wieringa, B., Mulders, S.A., et al. (2015). Cell membrane integrity in myotonic dystrophy type 1: implications for therapy. PLoS One *10*, e0121556.

51. Betts, C., Saleh, A.F., Arzumanov, A.A., Hammond, S.M., Godfrey, C., Coursindel, T., Gait, M.J., and Wood, M.J. (2012). Pip6-PMO, A new generation of peptide-oligonucleotide conjugates with improved cardiac exon skipping activity for DMD treatment. Mol. Ther. Nucleic Acids *1*, e38.

52. Holt, I., Mittal, S., Furling, D., Butler-Browne, G.S., Brook, J.D., and Morris, G.E. (2007). Defective mRNA in myotonic dystrophy accumulates at the periphery of nuclear splicing speckles. Genes Cells *12*, 1035–1048.

53. Burki, U., and Straub, V. (2017). Ultrasensitive hybridization-based ELISA method for the determination of phosphorodiamidate morpholino oligonucleotides in biological samples. Methods Mol. Biol. *1565*, 265–277.